FISEVIER

Contents lists available at ScienceDirect

### Journal of Alloys and Compounds

journal homepage: www.elsevier.com/locate/jalcom



## Layered *B*-site cation ordering: A key factor in ferrimagnetism of Y<sub>2</sub>MnCrO<sub>6</sub>



Lin Hao  $^{a,1}$ , Lei Yang  $^{b,1}$ , Ming-Hsien Lee  $^c$ , Tseh-Hsing Lin  $^c$ , ZhongFeng Zhang  $^a$ , XiangNan Xie  $^a$ , Hong Zhu  $^{a,*}$ 

- <sup>a</sup> Department of Physics, University of Science and Technology of China, Hefei, Anhui, China
- <sup>b</sup> Collaborative Innovation Center for Magnetoelectric Industry, China Three Gorges University, Yichang, Hubei, China
- <sup>c</sup> Department of Physics, Tamkang University, Taipei, Taiwan

#### ARTICLE INFO

# Article history: Received 17 January 2014 Received in revised form 19 February 2014 Accepted 20 February 2014 Available online 28 February 2014

Keywords:
Cr-doped manganite
X-ray diffraction
First-principles calculations
Ferrimagnetics
Semi-covalent exchange interaction

#### ABSTRACT

We report the Rietveld refinement of powder X-ray diffraction (XRD) pattern and first-principles calculations for the half- ${\rm Cr^{3+}}$  doped YMnO<sub>3</sub> compound. The Rietveld refinement results suggest that the compound has a monoclinic structure with the Mn<sup>3+</sup>/Cr<sup>3+</sup> layers alternately stacking along the [001] direction. The first-principles calculations show that the structure with layered *B*-site cation ordering has the lowest total energy; meanwhile, the insulating ferrimagnetic state is more favored compared to the ferromagnetic state, which is in agreement with the reported experimental results. Based upon Goodenough's model of semi-covalent exchange, we argue that the anisotropic magnetic couplings between the Mn<sup>3+</sup>/Cr<sup>3+</sup> cations ordered in layered pattern play an important role for the ferrimagnetism in the compound.

© 2014 Elsevier B.V. All rights reserved.

#### 1. Introduction

Since the discovery of high temperature superconductivity [1] and colossal magnetoresistance [2,3], perovskite oxides have attracted renewed interests for several decades because of a variety of properties they displayed, also including ferroelectricity [4] and multiferroics [5,6]. The prototype perovskite oxide has the generic formula  $ABO_3$  and structure with  $Pm\bar{3}m$  space group symmetry, in which the  $BO_6$  octahedra with corner-shared oxygen ions form a three dimensional network and the larger A-site cations sit in the 12-coordinate cubo-octahedral cavities. The basic structure of  $ABO_3$  is very flexible to tolerate various chemical substitutions onto all the three sites. Therefore, cation substitutions have been widely studied to expand the perovskite family and manipulate their physical properties from the beginning of the renewed research [7].

Besides cation substitution, recently it has been gradually understood that cation ordering, which can occur on either A- or B-site, is also an effective tailoring method for perovskite oxides. Among them, examples of A-site ordering are quite rare [8] and

most studies have focused on B-site ordered perovskites with the formula  $A_2BB'O_6$ , such as half-metallic  $Sr_2FeMoO_6$  [9], ferrimagnetic insulating  $La_2CrFeO_6$  [10] and ferromagnetic insulating  $A_2$ -MnNiO $_6$  (A = La, Bi) [11,12]. Depending on differences in radius and valence state of the B-site cations, there are three possible patterns for B-site cation ordering in perovskites [13]. The most common pattern is the rock salt ordering, in which each  $BO_6$  octahedron connects with six neighboring  $B'O_6$  octahedra. There are also a few examples of columnar ordering, which corresponds to 1D ordering because of connectivity of the  $BO_6$  octahedra in one dimension [14–16]. However, layered ordering (2D) with connectivity of the  $BO_6$  octahedra in two dimensions is extremely rare; the well known example is  $La_2CuSnO_6$  compound [17–20].

In our previous work, we found ferrimagnetism in half-doped YMn<sub>0.5</sub>Cr<sub>0.5</sub>O<sub>3</sub>, strongly suggesting the occurrence of *B*-site cation ordering in the compound, while the ordered pattern has not yet been identified [21]. By fitting the temperature dependence of inverse magnetic susceptibility in the paramagnetic state based upon the Curie–Weiss law, we also found that the local molecular field coefficient within the Cr<sup>3+</sup> sublattice is an unusual negative value and the cause remains unclear. In the present work, we reexamine the powder X-ray diffraction (XRD) pattern carefully by means of the Rietveld refinement. It is found that the layered *B*-site ordering with a monoclinic structure, where a = 5.2497(0) Å, b = 5.6401(1) Å, c = 7.4679(1) Å,  $\alpha = 89.97(8)^\circ$ , is more reasonable for the half-doped compound, which thus is denoted as Y<sub>2</sub>MnCrO<sub>6</sub>

<sup>\*</sup> Corresponding author. Address: Department of Physics, University of Science & Technology of China, 96 Jinzhai Road, Hefei, Anhui 230026, PR China. Tel.: +86 551 63600797; fax: +86 551 63601073.

E-mail address: zhuh@ustc.edu.cn (H. Zhu).

<sup>&</sup>lt;sup>1</sup> Lin Hao and Lei Yang contributed equally to this work.

(YMCO) hereafter. Employing the first-principles method, we compare the electronic structures and magnetic orders of YMCO with the three different B-site ordered patterns, and find that the ground state is a ferrimagnetic insulator, which is in agreement with the reported experimental results, with the alternative Cr/Mn ordered layers along the [001] direction. Based upon the layered B-site cation ordering, we explain the ferrimagnetic insulting state of YMCO in the framework of semi-covalent exchange model proposed by Goodenough [22], which demonstrates that the anisotropic magnetic coupling between  $\mathrm{Mn^{3^+}}(\mathrm{S}d^4)$  and neighboring  $\mathrm{Mn^{3^+}/Cr^{4^+}}(3d^3)$  cations plays a key role in the double perovskite YMCO.

#### 2. Technical details

YMCO ceramic sample was synthesized by solid state reaction. The room temperature XRD pattern, which was collected on Rigaku TTRAX III  $\theta/2\theta$  rotating anode XRD system with Cu K $\alpha$  radiation (1.5406 Å), indicated that the sample is a single phase of perovskite structure with corner-shared Mn/CrO $_6$  octahedra similar to YCrO $_3$ , rather than hexagonal YMnO $_3$ . YMCO shows an insulator behavior with high electrical resistivity and a ferrimagnetic transition at  $T_C \sim 75$  K. The details about synthesis, characterization and physical property measurements can be found elsewhere [21]. Powder XRD data collected from  $10^\circ$  to  $100^\circ$  with a step of  $0.02^\circ$  were refined by the Rietveld technique using GSAS-EXPGUI software [23]. The refined variables were scale factor, background, lattice parameters and peak profile function type 2.

The first-principles calculations described in this work were performed using the ultra-soft pseudopotential plane wave method and generalization gradient approximations (GGA) for exchange-correlation functions based on density-function theory (DFT), implemented in the Cambridge Serial Total Energy Package (CASTEP) [24,25]. The wave function was expanded in plane waves using a 400 eV energy cut-off. The reciprocal space integrations were carried out with a  $5 \times 4 \times 3$  Monkhorst-Pack *k*-point mesh. We performed structural optimization involving relaxation of the ionic positions as well as the cell shape and volume. The internal atomic coordinates were relaxed until force on each atom was smaller than 30 meV/Å. In the calculations, the tolerances for self-consistence were set at  $1.0 \times 10^{-6}$  eV/atom for total energy, 0.05~eV/Å for force,  $1.0\times10^{-5}~eV/\textrm{atom}$  for band energy, 0.05~GPafor maximum stress and 0.001 Å for the maximum displacement, respectively.

#### 3. Results and discussion

#### 3.1. Rietveld refinement for XRD pattern

The Rietveld refinement of powder XRD data at room temperature for the YMCO sample was performed in the monoclinic structure of the P2<sub>1</sub>/b space group with layered B-site cation ordering, in which  $Mn^{3+}$  and  $Cr^{3+}$  occupying 2b (0, 0, 0.5) and 2a (0, 0, 0) site, respectively. Fig. 1 shows the refinement result of powder XRD pattern for the YMCO sample. The observed, calculated, and difference patterns as well as the allowed reflections are displayed in the figure. One can see that the simulated result is in agreement with the experimental data. Note that there is a small diffraction peak at  $2\theta$  a little bit lower than 30°. In the present refinement with layered B-site ordering, the calculated (102)-diffraction position does correspond to this peak even the intensity is not matched so well, whereas this peak shifts to lower angle or totally absent in the calculated XRD patterns by using the B-site disordered or rock salt ordered structure [21]. Taken in this sense, it seems that the layered *B*-site order structure is superior to the others.

The main results of refinement, such as lattice parameters and atomic positions, are presented in the left column of Table 1,

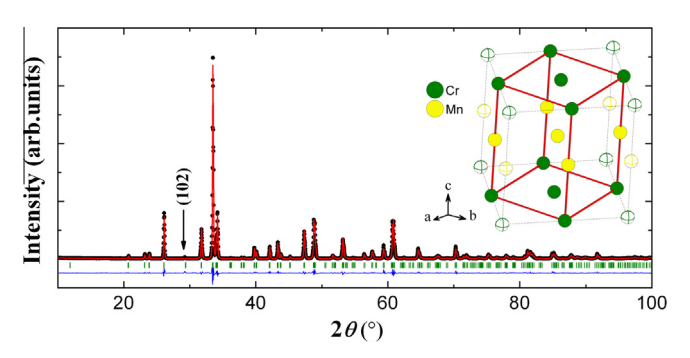


**Fig. 1.** Rietveld refinement of  $Y_2MnCrO_6$  XRD data with space group  $P2_1/b$  for Mn/Cr (001) layer ordered  $Y_2MnCrO_6$ . The experimental data are denoted as " $\bullet$ ", and the upper red solid line stands for the calculated data, the lower blue trace is the difference between observed and calculated patterns, and the short green bars in the middle are the positions of observed reflections calculated from the refined lattice parameters. The arrow which marks the location of (102)-peak is presented to guide the eyes. The structure schematic drawing of Mn/Cr (001) layer ordered  $Y_2MnCrO_6$  is placed on the right, where the Mn/Cr ions are represented by the yellow and green spheres, respectively, while the Y cations and O ions have been omitted for clarity. The superstructure corresponds to  $2a_c \times 2a_c \times 2a_c$  ( $a_c$  is a lattice parameter for a cubic perovskite) is indicated by the black dotted lines. (For interpretation of the references to colour in this figure legend, the reader is referred to the web version of this article.)

including the residuals for the weighted pattern  $R_{wp}$ , the pattern  $R_P$ , and the goodness of fit  $\chi^2$ . It can be seen that the refinement converged to a reliability factor of  $R_{wp} \sim 10.1\%$ . In the previous work [21], we compared the Rietveld refinement results of powder XRD by using the crystal structures with B-site disordered Pbnm and rock salt ordered  $P2_1/c$  space group, respectively, which gave similar reliability factors of  $R_{wp} \sim 11.7\%$ . Therefore, the XRD

**Table 1** Experimental (left column) and optimized (right column) lattice parameters and equilibrium atomic positions in the monoclinic  $P2_1/b$  structure of  $Y_2$ MnCrO<sub>6</sub>. The Wyckoff positions of the corresponding atoms are mentioned in brackets.

Lattice parameters       a       5.2497(0) Å       5.4072(0) Å         b       5.6401(1) Å       5.8423(0) Å         c       7.4679(1) Å       7.7121(1) Å         α       89.97(8)°       90.79(6)°         Atomic positions       Y (4e)         χ       0.9823(9)       0.9802(8)         y       -0.4250(3)       -0.4250(5)         z       0.2499(2)       0.2492(1)         Mn (2b)       χ       0         x       0       0         y       0       0         z       0.5       0.5         Cr (2a)       χ       0         x       0       0         y       0       0         z       0.6918(2)       0.6988(7)         y       -0.1673(9)       -0.2036(1)         z       0.0644(8)       0.0463(6)         O2 (4e)       χ       0.2983(2)       0.2953(3)         y       0.2043(5)       0.1810(4)         z       0.5440(5)       0.5483(7)		Experimental data <sup>a</sup>	Optimized data	
$\begin{array}{cccccccccccccccccccccccccccccccccccc$	Lattice parameters			
$\begin{array}{cccccccccccccccccccccccccccccccccccc$	а	5.2497(0) Å	5.4072(0) Å	
α       89.97(8)°       90.79(6)°         Atomic positions       Y (4e)         χ       0.9823(9)       0.9802(8)         y       -0.4260(3)       -0.4250(5)         z       0.2499(2)       0.2492(1)         Mn (2b)       χ       0       0         y       0       0       0         z       0.5       0.5       0.5         Cr (2a)       χ       0       0       0         y       0 <td>b</td> <td>5.6401(1) Å</td> <td>5.8423(0) Å</td>	b	5.6401(1) Å	5.8423(0) Å	
Atomic positions Y (4e) x	С		7.7121(1) Å	
Y (4e)  X	α	89.97(8)°	90.79(6)°	
x     0.9823(9)     0.9802(8)       y     -0.4260(3)     -0.4250(5)       z     0.2499(2)     0.2492(1)       Mn (2b)     x     0     0       x     0     0     0       y     0     0     0       z     0.5     0.5     0.5       Cr (2a)     x     0     0     0       y     0     0     0     0       z     0     0     0     0       01 (4e)     x     0.6918(2)     0.6988(7)     0       y     -0.1673(9)     -0.2036(1)     0.0463(6)       02 (4e)     x     0.2983(2)     0.2953(3)       y     0.2043(5)     0.1810(4)       z     0.5440(5)     0.5483(7)       03 (4e)	Atomic positions			
y       -0.4260(3)       -0.4250(5)         z       0.2499(2)       0.2492(1)         Mn (2b)       0       0         x       0       0       0         y       0       0       0         z       0.5       0.5       0         Cr (2a)       0       0       0         y       0       0       0         z       0       0       0         01 (4e)       0       0       0         x       0.6918(2)       0.6988(7)       0.6988(7)         y       -0.1673(9)       -0.2036(1)       0.0463(6)         02 (4e)       0       0       0         x       0.2983(2)       0.2953(3)         y       0.2043(5)       0.1810(4)         z       0.5440(5)       0.5483(7)         03 (4e)	Y (4e)			
z     0.2499(2)     0.2492(1)       Mn (2b)     0     0       x     0     0       z     0.5     0.5       Cr (2a)     0     0       x     0     0     0       y     0     0     0       z     0     0     0       01 (4e)     0.6918(2)     0.6988(7)     0.6988(7)       y     -0.1673(9)     -0.2036(1)     0.0463(6)       02 (4e)     0.0644(8)     0.0463(6)     0.0463(6)       02 (4e)     0.2983(2)     0.2953(3)     0.1810(4)       z     0.5440(5)     0.5483(7)     0.5483(7)       03 (4e)	X			
Mn (2b)  x 0 y 0 0 z 0.5 0.5 0.5  Cr (2a)  x 0 0 0 0 0 0 0 0 0 0 0 0 0 0 0 0 0 0	y			
x     0     0       y     0     0       z     0.5     0.5       Cr (2a)     0     0       x     0     0       y     0     0       z     0     0       01 (4e)     0     0       x     0.6918(2)     0.6988(7)       y     -0.1673(9)     -0.2036(1)       z     0.0644(8)     0.0463(6)       02 (4e)     0       x     0.2983(2)     0.2953(3)       y     0.2043(5)     0.1810(4)       z     0.5440(5)     0.5483(7)       03 (4e)	Z	0.2499(2)	0.2492(1)	
y     0     0       z     0.5     0.5       Cr (2a)     0     0       x     0     0     0       y     0     0     0       01 (4e)     0.6918(2)     0.6988(7)     0.6988(7)       y     -0.1673(9)     -0.2036(1)     0.0463(6)       y     0.0644(8)     0.0463(6)     0.0463(6)       O2 (4e)     0.2983(2)     0.2953(3)     0.1810(4)       y     0.2043(5)     0.1810(4)     0.5483(7)       O3 (4e)	Mn (2b)			
z     0.5     0.5       Cr (2a)     0     0       x     0     0     0       y     0     0     0       O1 (4e)     0     0     0       x     0.6918(2)     0.6988(7)     0       y     -0.1673(9)     -0.2036(1)     0.0463(6)       D2 (4e)     0.0463(6)     0       x     0.2983(2)     0.2953(3)       y     0.2043(5)     0.1810(4)       z     0.5440(5)     0.5483(7)       O3 (4e)	x	0	0	
Cr (2a)  x  0  y  0  c  0  0  0  0  0  0  0  0  0  0  0	y	0	0	
x     0     0       y     0     0       z     0     0       O1 (4e)     0.6918(2)     0.6988(7)       y     -0.1673(9)     -0.2036(1)       z     0.0644(8)     0.0463(6)       O2 (4e)     0.2983(2)     0.2953(3)       y     0.2043(5)     0.1810(4)       z     0.5440(5)     0.5483(7)       O3 (4e)	Z	0.5	0.5	
y     0     0       z     0     0       O1 (4e)         x     0.6918(2)     0.6988(7)       y     -0.1673(9)     -0.2036(1)       z     0.0644(8)     0.0463(6)       O2 (4e)         x     0.2983(2)     0.2953(3)       y     0.2043(5)     0.1810(4)       z     0.5440(5)     0.5483(7)       O3 (4e)	Cr (2a)			
z 0 0 0  O1 (4e) x 0.6918(2) 0.6988(7) y -0.1673(9) -0.2036(1) z 0.0644(8) 0.0463(6)  O2 (4e) x 0.2983(2) 0.2953(3) y 0.2043(5) 0.1810(4) z 0.5440(5) 0.5483(7)  O3 (4e)	X	0	0	
O1 (4e)       x     0.6918(2)     0.6988(7)       y     -0.1673(9)     -0.2036(1)       z     0.0644(8)     0.0463(6)       O2 (4e)     x     0.2983(2)     0.2953(3)       y     0.2043(5)     0.1810(4)       z     0.5440(5)     0.5483(7)       O3 (4e)	y	0	0	
x     0.6918(2)     0.6988(7)       y     -0.1673(9)     -0.2036(1)       z     0.0644(8)     0.0463(6)       O2 (4e)     x     0.2983(2)     0.2953(3)       y     0.2043(5)     0.1810(4)       z     0.5440(5)     0.5483(7)       O3 (4e)	Z	0	0	
y -0.1673(9) -0.2036(1) z 0.0644(8) 0.0463(6) O2 (4e) x 0.2983(2) 0.2953(3) y 0.2043(5) 0.1810(4) z 0.5440(5) 0.5483(7)	01 (4e)			
z 0.0644(8) 0.0463(6)  O2 (4e) x 0.2983(2) 0.2953(3) y 0.2043(5) 0.1810(4) z 0.5440(5) 0.5483(7)  O3 (4e)	X		0.6988(7)	
O2 (4e)  x	y	` ,	` '	
x     0.2983(2)     0.2953(3)       y     0.2043(5)     0.1810(4)       z     0.5440(5)     0.5483(7)       O3 (4e)	Z	0.0644(8)	0.0463(6)	
y 0.2043(5) 0.1810(4) z 0.5440(5) 0.5483(7) 03 (4e)	O2 (4e)			
z 0.5440(5) 0.5483(7) O3 (4e)	x			
O3 (4e)	y		` '	
, ,	Z	0.5440(5)	0.5483(7)	
	O3 (4e)			
	X	0.1104(2)	0.0935(1)	
y = -0.0399(6) -0.0250(4)	y			
z 0.2552(4) 0.2475(5)	Z	0.2552(4)	0.2475(5)	

<sup>&</sup>lt;sup>a</sup> Reliability factors are  $R_{wp}$  = 10.11%,  $R_P$  = 7.27% and  $\chi^2$  = 1.462.

analysis left a question open for the *B*-site cation ordering in the YMCO compound, even though the ferrimagnetism of the compound strongly implies this point. In this work, however, the refinement reliability  $R_{wp}$  decreases substantially from  $\sim 11.7\%$  to 10.1% for the structure with layered *B*-site cation ordering. Combining with the improvement of (102) diffraction peak mentioned above, now we consider that the layered *B*-site ordered pattern is more reasonable in the YMCO perovskite.

As shown in the inset of Fig. 1, the monoclinic structure of YMCO can be viewed as a distorted orthogonal structure. The MnO<sub>6</sub> and CrO<sub>6</sub> octahedral layers alternately stack along the *c* axis. Considering the similarity of YMCO and layered ordered La<sub>2</sub>CuSnO<sub>6</sub>, we expanded the refined cell to a superstructure corresponds to  $2a_c \times 2a_c \times 2a_c$  ( $a_c$  is a lattice parameter for a cubic perovskite) [17]. The expanded lattice gives a triclinic structure with  $a_s = 7.7054 \text{ Å}$ ,  $b_s = 7.7054 \text{ Å}$ ,  $c_s = 7.4683 \text{ Å}$ , and  $\alpha = 89.971^\circ$ ,  $\beta$  = 90.029°,  $\gamma$  = 94.108°. As the similar axes along which the  $BO_6$ and B'O<sub>6</sub> octahedral layers alternately stack, it is noteworthy that the  $c_s$  axis in YMCO is considerably shorter than the  $a_s$  and  $b_s$  axes, whereas it is the longest in La<sub>2</sub>CuSnO<sub>6</sub> compound, which has been attributed to the alignment of Jahn-Teller axes of CuO6 octahedra along this axis [17]. The reason for lattice contraction of the  $c_s$  in YMCO will be discussed below by considering the difference between Mn/Cr-O bond types along the three directions.

#### 3.2. First-principles calculations for three B-site ordered patterns

For comparison, based on the obtained lattice parameters, we rearrange B-site cations to form rock salt, column and layered patterns of ordering, which are also denoted as (111), (110) and (001) ordering, respectively [26]. Firstly, the geometric structure optimization was performed for the three B-site ordering patterns by using BFGS (Broyden–Fletcher-Goldfarb–Shanno) method [27,28], which gave that the cell parameters are slightly overestimated with errors of  $\sim$  3.0%. For comparison with the experimental data, the optimized structural parameters of (001) ordering model including the lattice parameters and equilibrium atomic positions are given in the right column of Table 1, which shows that the structure optimization is acceptable.

After that, we calculated total energies, energy gaps and magnetic moments for the three ordered patterns with ferromagnetic (FM) or ferrimagnetic (FiM) state. Table 2 summarizes the calculated results. Without regard to magnetic states, it can be seen that the (001) B-site ordered patterns have the lowest energies of all the combinations tried, while the (111) ordered pattern with FiM state has the highest energy. The result is different from the most double perovskite  $A_2BB'O_6$ , where the rock salt type (111) ordering is the most common pattern [29,30]. As an exception,  $La_2CuSnO_6$  has a layered B-site ordered structure, which is stabilized by a first order Jahn–Teller distortion of the  $Cu^{2+}$  cations and the appropriate degree of octahedral tilting [13]. In the present case,  $Mn^{3+}$  cation is also a typical Jahn–Teller ion, so that the B-site

**Table 2** Total energy (relative to (001) FiM state), band gap, total magnetization of  $Y_2MnCrO_6$  per formula unit (f.u.) and approximate spin-only moments of Cr/Mn ions for each structure.

Mn/Cr order	$E_{tot}$ (eV)	$E_g$ (eV)	Moment (µ <sub>B</sub> )		
			Formula unit	Mn	Cr
(001) FiM	0	0.47	1	3.8	-3.04
(001) FM	0.011	0.44	7	3.84	3.08
(110) FiM	0.09	0	1.2	3.86	-2.88
(110) FM	0.05	0.11	7	3.92	3.02
(111) FiM	0.135	0.02	1	3.72	-2.9
(111) FM	0.074	0.33	7	3.9	3.04

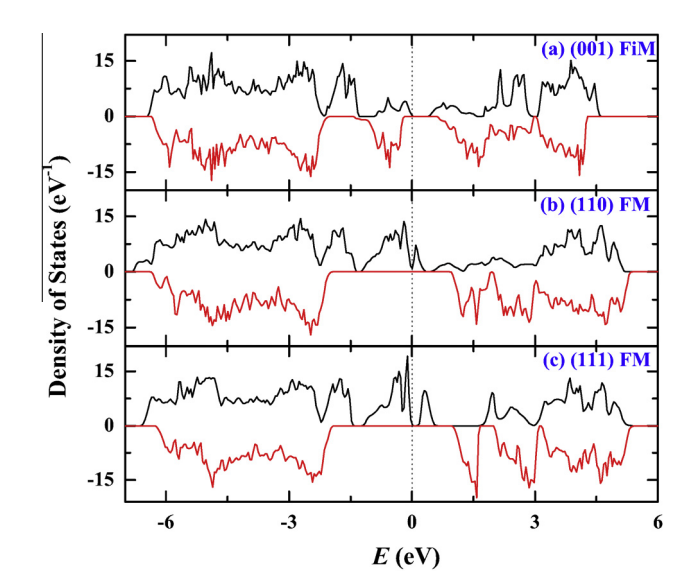
cation ordering in the YMCO compound is reasonable. In the (001) ordering, the energy for FiM state is lower than that for FM state, clearly indicating that the (001) *B*-site cation ordered structure with ferrimagnetic order is the ground state for the YMCO compound. As for the (110) and (111) ordered patterns, it can be seen in Table 2 that FM state has lower energy than FiM state, indicating FM state is more stable, which is in contrast to the experimental results [21].

Fig. 2 displays the total densities of states (TDOS) for the three B-site ordered patterns with relatively lower total energy. It can be seen that the (001) FiM state has an energy gap ( $E_g$ ) of 0.47 and 0.76 eV for the spin-up and spin-down bands, respectively, and the Fermi level ( $E_F$ ) slightly above the valence band lies in the energy gap, so it behaves like a typical semiconductor as we reported before [21]. For the (110) and (111) FM states, the semiconductor behavior remains, but the energy gap distinctly decreases to 0.11 and 0.33 eV, respectively.

Focusing on the (001) FiM state, we show its spin-dependent total and partial DOS of each element in Fig. 3. In the vicinity of the Fermi level, one can see that the total DOS of spin-up and spin-down bands are governed by the Mn and Cr 3d states, respectively. The energy splitting between  $t_{2g}$  and  $e_g$  states due to crystalline field is in the range 1-1.5 eV, which is much lower than the exchange splitting  $\sim$  3 eV, so the high spin states for both of the Mn and Cr cations are expected. The calculated magnetic moments give the values of 3.8 and 3.04  $\mu_B$  (see Table 2) for Mn and Cr cations, respectively, which are slightly different from 4 and 3  $\mu_B$  for  $Mn^{3+}$  (3d<sup>4</sup>) and  $Cr^{3+}$  (3d<sup>3</sup>) ions with high spin state. The reason is due to the hybridization between the Mn/Cr 3d states and O 2p state, because there is a minority distribution of O 2p band at energies around  $E_F$  as shown in Fig. 3. It is also noteworthy that the calculated magnetic moment of 1  $\mu_B/f.u.$  for the (001) FiM state is in good agreement with the experimental value [21].

#### 3.3. Semi-covalent exchange interaction in YMCO

Up to now we have found out that the layered *B*-site cation ordered ferrimagnetism is the ground state for the YMCO compound. Next, let us consider a possible mechanism to understand such a ground state. Generally speaking, there are three kinds of indirect exchange interaction between two magnetic cations separated by an anion, which are superexchange [31,32]/double exchange



**Fig. 2.** Total densities of states (DOS) of the three model structures for *B*-site ordered Y<sub>2</sub>MnCrO<sub>6</sub>. The Fermi energy sets to zero.

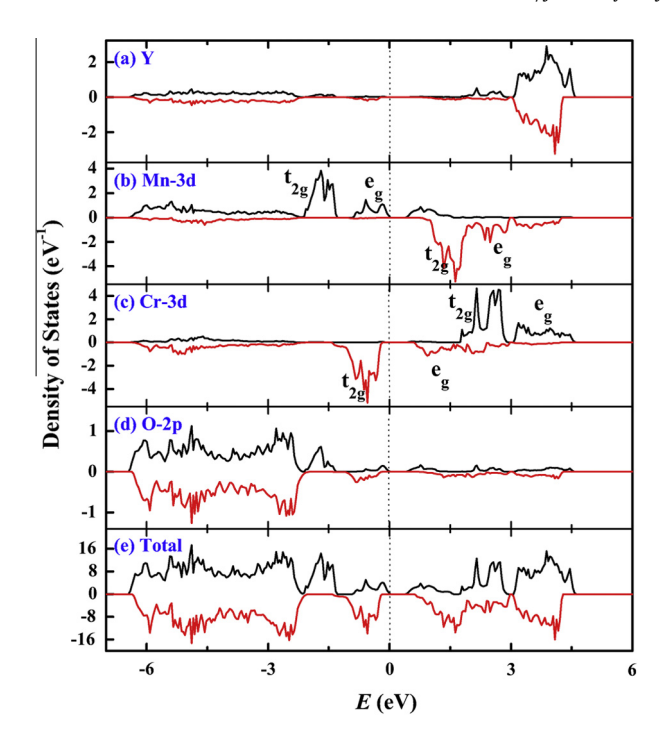


**Fig. 3.** Projected and total densities of states (DOS) of Cr/Mn (001) ordered  $Y_2MnCrO_6$ . The Fermi energy sets to zero. (a) Projected DOS of Y, (b) partial DOS of Mn 3d, (c) partial DOS of Cr 3d, (d) partial DOS of O 2p, and (e) total DOS.

[33,34] mediated by virtual/real electron transfers and semi-covalent exchange [35] depending upon the concept of semi-covalent bonding. Because YMCO displays an insulator behavior till low temperatures, the double exchange interaction can be ruled out in the present case. As for the superexchange interaction, it is somewhat too primitive to give correct predictions in manganese oxides. Therefore, we choose the semi-covalent exchange as the possible mechanism in the YMCO compound.

According to the semi-covalent exchange model proposed by Goodenough [22], if both the transition metal cations extend their hybrid orbitals towards the same  $O^{2-}$  ion forming two semi-covalent bonds, they are antiferromagnetically coupled; if only one semi-covalent bond and another ionic bond, the two cations are ferromagnetically coupled. Fig. 4 displays the sketch of structures and semi-covalent exchange interactions for (a) LaMnO<sub>3</sub>, (b) YMCO ordered in the rock salt pattern and (c) YMCO ordered in the layered pattern. Mn<sup>3+</sup> (3 $d^4$ ) cation hybridizes square ( $dsp^2$ ) lattice orbitals, which are strongly anisotropic along the three axes. In LaMnO<sub>3</sub> as shown in Fig. 4(a), two hybrid orbitals of Mn<sup>3+</sup> cations point toward the same  $O^{2-}$  ion along the  $c_s$ -axis, so that the two

Mn<sup>3+</sup> cations are antiferromagnetically coupled along this direction. Whereas in the  $a_s$ - $b_s$  plane, only one semi-covalent bond collaborating with one ionic bond leads to a ferromagnetic coupling between the Mn<sup>3+</sup> cations. As a result, LaMnO<sub>3</sub> has an A-type antiferromagnetic ground state consistent with the experimental results reported by Wollan and Koehler [35]. Considering Mn<sup>4+</sup>/Cr<sup>3+</sup> cations with an outer-electron configuration  $3d^3$ , they hybridize octahedral  $(d^2sp^3)$  orbitals, which can therefore point simultaneously toward all the six neighboring O<sup>2-</sup> anions. If we arrange B-site cations of YMCO in the rock salt (111) ordered pattern as shown in Fig. 4(b), beginning with the lower left Cr<sup>3+</sup>(1) cation, it will be coupled ferromagnetically with the nearest-neighboring  $Mn^{3+}$  cations along the  $a_s$ -axis and antiferromagnetically along the  $b_s/c_s$ -axis, respectively, which means that a ferromagnetic Mn<sup>3+</sup> sublattice is out of the question. Furthermore, the spin orientation of the next-nearest-neighboring Cr<sup>3+</sup> cations is totally vague. For example, the upper middle Cr<sup>3+</sup>(2) cation should be spin-down due to the antiferromagnetic coupling along the  $c_s$ -axis; meanwhile, it should be spin-up according to the ferromagnetic coupling along the  $b_s$ -axis. Finally, the spin orientation of the upper right Mn<sup>3+</sup>(1) cation remains a big question mark. As a result, the rock salt (111) ordered pattern of B-site cation is irrational for the YMCO compound. Actually, half-doped La<sub>0.5</sub>Ca<sub>0.5</sub>MnO<sub>3</sub> is a CE-type antiferromagnetism with charge ordering in the (110) column pattern [35]. However, it is obvious that such a structure is improper to the ferrimagnetic state in YMCO compound.

Next, we consider the layered B-site cation ordering as a prerequisite for the ferrimagnetism in YMCO. As shown in Fig. 4(c), Mn<sup>3+</sup> and Cr<sup>3+</sup> cations are antiferromagnetically coupled because both of them share a semi-covalent bond with  $O^{2-}$  anion along the  $c_s$ -axis, while  $Mn^{3+}$  cations within the  $a_s-b_s$  plane are ferromagnetically coupled due to single semi-covalent bond with the intermediate anion as in LaMnO<sub>3</sub> compound. It is noteworthy that Cr<sup>3+</sup> cations within the  $a_s$ - $b_s$  plane are antiferromagnetically coupled according to the semi-covalent exchange model. In our previous work [21] by fitting the temperature dependence of inverse susceptibility in the paramagnetic state according to the Curie-Weiss law, actually we found a negative local molecular field coefficient in the Cr<sup>3+</sup> sublattice, which is coincident with the present picture. Goodenough has also pointed out that the separation between two cations connected with the same O<sup>2-</sup> anion by one semi-covalent bond and one ionic bond is large, while it is the smallest when both of them form semi-covalent bonds with the anion [22]. In our case, the superstructure reveals that the c<sub>s</sub>-axis, along which MnO<sub>6</sub> and CrO<sub>6</sub> octahedral layers are stacked alternately, is the shortest, indicating that Cr3+ and Mn3+ cations are strongly antiferromagnetically coupled via. two semi-covalent bonds sharing the same O<sup>2-</sup> anion. So in contrast to La<sub>2</sub>CuSnO<sub>6</sub>, the lattice contraction of the  $c_s$ -axis in YMCO is rational in the semi-covalent exchange scenario. On the other hand, the  $a_s$ - and  $b_s$ -axis are longer, accordingly

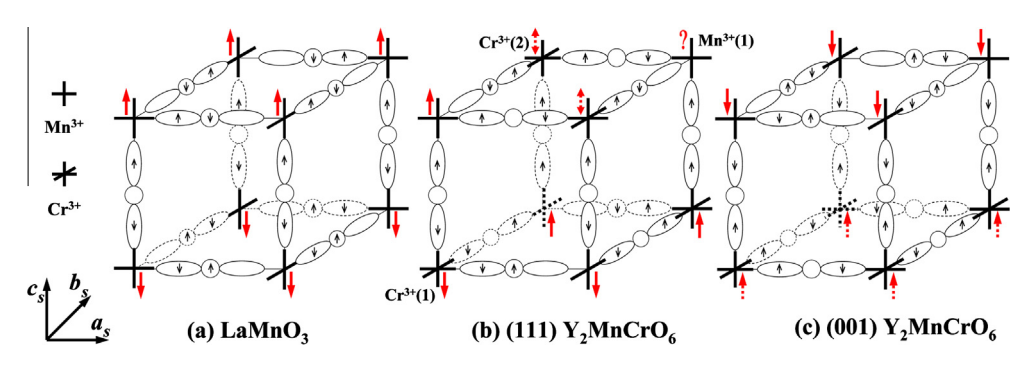


Fig. 4. The schematics of crystal structures and Goodenough's semi-covalent exchange interactions for (a) LaMnO<sub>3</sub>, (b) Y<sub>2</sub>MnCrO<sub>6</sub> ordered in rock salt pattern and (c) Y<sub>2</sub>MnCrO<sub>6</sub> ordered in layered pattern.

the antiferromagnetic exchange between  $Cr^{3+}$  cations within the  $a_s$ – $b_s$  plane are restrained. With the help of the strongest antiferromagnetic exchange interaction between  $Cr^{3+}/Mn^{3+}$  cations and bigger ferromagnetic  $Mn^{3+}$  sublattice,  $Cr^{3+}$  sublattice are ferromagnetic ordered even with the antiferromagnetic coupling between  $Cr^{3+}$  cations. As a result, the YMCO compound with B-site cations ordered in layered pattern enters into a ferrimagnetic ground state.

#### 4. Conclusions

In summary, the Rietveld refinement of powder XRD pattern shows that the double perovskite structure with a layered *B*-site cation ordered pattern is more reliable for the YMCO compound. We have used the first-principles calculations to compute the electronic structures with different *B*-site ordered patterns and magnetic orders for comparison. The calculation results indicate that the insulating ferrimagnetism with (001) layered pattern for *B*-site cation ordering is the ground state for the system, which is in agreement with the experimental results. We provide a discussion in the framework of semi-covalent exchange mechanism to understand the anisotropic magnetic coupling between Cr<sup>3+</sup>/Mn<sup>3+</sup> cations as well as ferrimagnetic order in the system. Our results reveal that the layered pattern of *B*-site cation ordering plays a key role for the ferrimagnetism in the YMCO double perovskite oxide.

#### Acknowledgement

We would like to thank Prof. Luyuan Hao for valuable discussion and technical help during the first-principles calculations. This work is supported by the National Nature Science Foundation of China (Grant No. 11174261).

#### References

- [1] J.G. Bednorz, K.A. Muller, Z. Phys. B-Condens. Mater. 64 (1986) 189–193.
- [2] R. von Helmolt, J. Wecker, B. Holzapfel, L. Schultz, K. Samwer, Phys. Rev. Lett. 71 (1993) 2331–2333.
- [3] S. Jin, T.H. Tiefel, M. McCormack, R.A. Fastnacht, R. Ramesh, L.H. Chen, Science 264 (1994) 413–415.
- [4] R.E. Cohen, Nature 358 (1992) 136–138.
- [5] T. Kimura, T. Goto, H. Shintani, K. Ishizaka, T. Arima, Y. Tokura, Nature 426 (2003) 55–58.

- [6] J. Wang, J.B. Neaton, H. Zheng, V. Nagarajan, S.B. Ogale, B. Liu, D. Viehland, V. Vaithyanathan, D.G. Schlom, U.V. Waghmare, N.A. Spaldin, K.M. Rabe, M. Wuttig, R. Ramesh, Science 299 (2003) 1719–1722.
- [7] B. Raveau, A. Maignan, C. Martin, M. Hervieu, Chem. Mater. 10 (1998) 2641– 2652.
- [8] S.V. Trukhanov, A.V. Trukhanov, H. Szymczak, R. Szymczak, M. Baran, J. Phys. Chem. Solids 67 (2006) 675–681.
- [9] D.D. Sarma, P. Mahadevan, T. Saha-Dasgupta, S. Ray, A. Kumar, Phys. Rev. Lett. 85 (2000) 2549–2552.
- [10] S. Chakraverty, A. Ohtomo, D. Okuyama, M. Saito, M. Okude, R. Kumai, T. Arima, Y. Tokura, S. Tsukimoto, Y. Ikuhara, M. Kawasaki, Phys. Rev. B 84 (2011) 064436.
- [11] M. Azuma, K. Takata, T. Saito, S. Ishiwata, Y. Shimakawa, M. Takano, J. Am. Chem. Soc. 127 (2005) 8889–8892.
- [12] S.F. Matar, M.A. Subramanian, A. Villesuzanne, V. Eyert, M.H. Whangbo, J. Magn. Magn. Mater. 308 (2007) 116–119.
- [13] G. King, P.M. Woodward, J. Mater. Chem. 20 (2010) 5785-5796.
- [14] V. Caignaert, F. Millange, M. Hervieu, E. Suard, B. Raveau, Solid State Commun. 99 (1996) 173–177.
- [15] P.G. Radaelli, D.E. Cox, M. Marezio, S.W. Cheong, Phys. Rev. B 55 (1997) 3015–3023.
- [16] P.M. Woodward, T. Vogt, D.E. Cox, A. Arulraj, C.N.R. Rao, P. Karen, A.K. Cheetham, Chem. Mater. 10 (1998) 3652–3665.
- [17] M.T. Anderson, K.R. Poeppelmeier, Chem. Mater. 3 (1991) 476-482.
- [18] M.T. Anderson, K.R. Poeppelmeier, S.A. Gramsch, J.K. Burdett, J. Solid State Chem. 102 (1993) 164–174.
- [19] M. Azuma, S. Kaimori, M. Takano, Chem. Mater. 10 (1998) 3124-3130.
- [20] A. Masuno, M. Haruta, M. Azuma, H. Kurata, S. Isoda, M. Takano, Y. Shimakawa, Appl. Phys. Lett. 89 (2006) 211913.
- [21] L. Yang, Q.Y. Duanmu, L. Hao, Z.F. Zhang, X.P. Wang, Y.Y. Wei, H. Zhu, J. Alloys Comp. 570 (2013) 41–45.
- [22] J.B. Goodenough, Phys. Rev. 100 (1955) 564-573.
- [23] A.C. Larson, R.B. Von Dreele, Los Alamos Natl. Lab. Rep. (2004) 86-748.
- [24] M.C. Payne, M.P. Teter, D.C. Allan, T.A. Arias, J.D. Joannopoulos, Rev. Mod. Phys. 64 (1992) 1045–1097.
- [25] S.J. Clark, M.D. Segall, C.J. Pickard, P.J. Hasnip, M.J. Probert, K. Refson, M.C. Payne, Z. Kristallogr. 220 (2005) 567–570.
- [26] M. Zhu, Y. Lin, E.W.C. Lo, Q. Wang, Z.J. Zhao, W.H. Xie, Appl. Phys. Lett. 100 (2012) 062406.
- [27] J. Bonnans, J. Gilbert, C. Lemaréchal, C. Sagastizbál, Numerical Optimization Theoretical and Practical Aspects, Springer, 2006.
- [28] G.P. Francis, M.C. Payne, Finite basis set corrections to total energy pseudopotential calculations, J. Phys.: Condens. Matter 2 (1990) 4395–
- [29] M.W. Lufaso, P.W. Barnes, P.M. Woodward, Acta Crystallogr. Sect. B-Struct. Sci. 62 (2006) 397–410.
- [30] C.J. Howard, B.J. Kennedy, P.M. Woodward, Acta Crystallogr. Sect. B-Struct. Sci. 59 (2003) 463-471.
- [31] H.A. Kramers, Physica 1 (1934) 182-192.
- [32] P.W. Anderson, Phys. Rev. 79 (1950) 350–356.
- [33] C. Zener, Phys. Rev. 82 (1951) 403-405.
- [34] P.G. de Gennes, Phys. Rev. 118 (1960) 141-154.
- [35] E.O. Wollan, W.C. Koehler, Phys. Rev. 100 (1955) 545-563.